

ONGOING ANALYSES OF ROCKET BASED COMBINED CYCLE ENGINES BY THE APPLIED FLUID DYNAMICS ANALYSIS GROUP AT MARSHALL SPACE FLIGHT CENTER

Joseph H. Ruf, James B. Holt, Francisco Canabal
Marshall Space Flight Center

ABSTRACT

This paper presents the status of analyses on three Rocket Based Combined Cycle (RBCC) configurations underway in the Applied Fluid Dynamics Analysis Group (TD64). TD64 is performing computational fluid dynamics (CFD) analysis on a Penn State RBCC test rig, the proposed Draco axisymmetric RBCC engine and the Trailblazer engine. The intent of the analysis on the Penn State test rig is to benchmark the Finite Difference Navier Stokes¹ (FDNS) code for ejector mode fluid dynamics. The Draco analysis was a trade study to determine the ejector mode performance as a function of three engine design variables. The Trailblazer analysis is to evaluate the nozzle performance in scramjet mode. Results to date of each analysis are presented

NOMENCLATURE

A_s = Secondary Flow Area
 A_p = primary thruster exit flow area plus thruster base area
 A_5 = mixer inlet area, $A_s + A_p$
 A_8 = ram burner area
 D = mixer diameter at mixer inlet
 L = mixer length
 R = radius
 y = local radius
 \dot{m} = mass flow rate

SUMMARY

Three analyses related to RBCC concepts are underway in TD64 at MSFC. Each analysis is described in its own section of this paper. The first two analyses deal with the first mode of the RBCC engines or the 'ejector' mode. The ejector mode occurs at Mach numbers less than one while the primary thruster exhaust entrains or 'ejects' air through the engine.

The first analysis is a benchmark of the FDNS CFD code for RBCC ejector mode fluid physics. Penn State University (PSU) is in the process of completing a benchmark quality laboratory experiment of an RBCC

configuration in ejector mode. This benchmark will determine how best to use FDNS to predict ejector mode performance of RBCC engine concepts.

The second analysis used FDNS to predict the ejector mode performance of an early configuration of the Darco RBCC engine. A trade study of 27 engine configurations was performed. Draco is a near term RBCC axisymmetric engine intended to air-breathe up through the ramjet mode.

The third analysis is using FDNS to determine the nozzle performance for the Trailblazer vehicle in the scramjet mode. The computational domain begins inside the engine and includes the freestream flow for the installed performance effects. The Trailblazer vehicle is single-stage-to-orbit RBCC concept with three semi-axisymmetric engines.

FDNS EJECTOR FLOW BENCHMARKING

INTRODUCTION

The PSU RBCC hardware is a two-dimensional design (figure 1) with variable geometry to enable studies of RBCC mixing and secondary combustion phenomena. Gaseous hydrogen and oxygen were used as propellants. The ejector mode configuration had a simple two-dimensional inlet and exhausted to atmospheric pressure. The ejector mode test included measurements for wall static pressure, wall heat flux and overall thrust. Additionally, optical and laser based diagnostics were employed to evaluate mixing and secondary combustion during testing. A primary objective of the PSU ejector mode test was to provide high quality benchmark data for CFD code validation.

OBJECTIVE

The objective of this analysis is to benchmark the FDNS CFD code for RBCC ejector mode operation. The key physical process of interest is the shear layer interaction between and mixing of the primary thruster exhaust with the secondary (air) flow. This process has a significant affect on the amount of secondary flow entrained and, therefore, the performance of the RBCC's ejector mode.

APPROACH

The test conditions modeled are for the primary thruster at 500 psi and an oxidizer-to-fuel (O/F) ratio of eight. The afterburner has a small amount of gaseous hydrogen injected. A semi-3D domain is currently being used to model the test hardware. The symmetry in the hardware allows the domain to contain only 1/4th of the hardware flowpath. The semi-3D domain is fairly dense in the axial and vertical directions, but is coarse in depth. The depth is incorporated to enable the afterburner fuel injection. The analysis is steady state and implements finite-rate chemistry and thermodynamics and the standard k-ε turbulence model.

STATUS

The only test data currently available is the upper wall static pressures for two runs. The complete data should be available with a few weeks. The wall pressures from the current solution are compared to the test data in figure 2. The semi-3D results match the test data very well. The slight drop in pressure in the afterburner is due to the hydrogen injection and afterburning. All hydrogen is consumed before the gases exit the nozzle.

FUTURE WORK

Future work will involve refining the three-dimensional grid and then comparing to the complete experimental data set for O/F of eight. Further benchmarking will be pursued by modeling the same hardware with the primary thruster at an O/F of four.

DRACO EJECTOR/MIXER TRADE STUDY

INTRODUCTION

The first or ‘ejector’ mode of the Draco engine will have a significant impact on the overall engine cycle performance. By their very nature the one-dimensional RBCC cycle performance codes used for RBCC conceptual design do not capture the multidimensional fluid dynamic interactions that may have significant effects on the ejector mode performance. If CFD can be integrated into the design process early the RBCC cycle performance codes would benefit from information on the three-dimensional effects and engine designers would gain additional understanding of RBCC internal fluid dynamics.

An early Draco configuration was chosen to start the CFD trade study on ejector/mixer performance even though significant changes in the Draco design were likely. This trade study was used to get all the CFD related tools in place, working and streamlined so future ejector/mixer configuration trade studies could be tackled much quicker.

OBJECTIVE

The first objective to this analysis was to determine the Draco ejector/mixer performance trends for quiescent freestream for a matrix of engine design variables. The second objective was to get the CFD and related analysis tools in place, working and streamlined for quick turn-around of ejector/mixer configuration trade studies.

APPROACH

The Draco flowpath configuration for this analysis was axisymmetric with a single primary thruster on the engine centerline (figure 3). The primary thruster was housed in a centerbody that created an annular constant area inlet. On the front of the centerbody was an inlet compression spike.

Figure 3 defines some of the Draco design variables. The ejector/mixer inlet plane is defined to be the exit plane of the primary thruster. The mixer length (L) was a function of two of the trade space variables, L/D and A_s/A_p . The mixer diameter (D) was defined as its diameter at the inlet plane. A_s is the area of the secondary flow area and A_p is the area of the primary thruster exit area plus any base area surrounding the thruster. A_5 is the total flow area at the ejector/mixer inlet plane ($A_s + A_p$) and A_8 is the flow area of the ram burner.

The engine design variables that defined the trade space were: ejector/mixer L/D; A_s/A_p , the ratio of secondary to primary flow areas; and A_8/A_5 , ratio of ram burner to ejector/mixer inlet areas. Each variable had three values so that the trade space included 27 cases as shown in table 1. Several of the engine configurations are shown in figure 4.

The performance of the ejector/mixer was measured with the following figures of merit (FOM): By-pass ratio, the ratio of secondary flow to primary flow; ejector compression ratio (ECR), the ratio of total pressure at ejector/mixer exit to total pressure of secondary flow; ejector/mixer thrust efficiency, thrust at the exit divided by thrust at the mixer inlet; ejector/mixer mixing efficiency as defined below.

$$\text{Mixer Mixing Efficiency} \equiv 1 - \frac{\sum_{y=0}^{R_{exit}} |\dot{m}'_{air \text{ ideal}} - \dot{m}'_{air @ y}|_{\text{mixer exit}}}{\sum_{y=0}^{R_{inlet}} |\dot{m}'_{air \text{ ideal}} - \dot{m}'_{air @ y}|_{\text{mixer inlet}}}$$

The mixing efficiency was defined as a measure of how well the mixer achieved perfectly mixed homogeneous flow at the ejector/mixer exit. The mass flow distribution of secondary flow (air) was used to

calculate the mixing efficiency. The difference between homogeneous flow and the air mass flow distribution that existed at the ejector/mixer inlet was determined and normalized to represent zero mixing. A value of 1 would occur only if the entrained air was perfectly mixed with the primary flow and the resulting mixed flow had no gradients ('plug' flow). Values of less than zero were possible if the ejector/mixer increased the striation of the primary and secondary flows.

The geometric definition of the 27 cases was extracted from an engine design spreadsheet. This geometry was passed to Gridgen⁵ to generate the grids. All grids contained the same number of nodes in the freestream, inlet, ram burner and nozzle portions of the domain. The number of nodes in the axial direction of the ejector/mixer varied because of their different lengths. A consistent axial delta-s was used in the ejector/mixer region. The grids contained approximately 33k, 38k and 44k nodes for the L/D=1, 2, and 3 configurations, respectively. Once the Gridgen template was in place for each L/D grids the 24 subsequent grids could be generated in less than five minutes each.

The FDNS CFD code was implemented with a two-specie model: air and a specie of average hot-gas properties. This analysis was non-reacting but future analysis will include finite rate reaction as necessary. The standard k-ε turbulence model was implemented. The benchmarking effort above will indicate if another turbulence model is more appropriate for future work.

The freestream far field boundaries were set to conserve total pressure of one atmosphere. All engine surfaces were set to no-slip adiabatic walls and the centerline of the engine was set to an axisymmetric boundary condition. Primary thruster mass flow rates were the same for all configurations but each A_s/A_p ratio resulted in a different primary thruster area ratio, therefore, a different primary thruster exit pressure. The $A_s/A_p=1$ had the lowest exit pressure and $A_s/A_p=3$ had the highest exit pressure. The primary thruster exit flow properties were calculated with the Reacting and Multiphase Program⁴. These thruster exit flow properties were defined as fixed inlet conditions for the ejector/mixer analysis.

The solution procedure was highly automated by using a series of Unix scripts. The scripting automatically acquired the appropriate grid and initialized the grid and solution in FDNS format. The scripts then ran the solution 15 thousand iterations through a series of CFD inputs increasing the time step while decreasing the damping. The grid was then adapted based on flow field gradients with Self-Adaptive Grid Code⁵, the solutions were run 15 thousand more iterations, and post processed for the FOMs. Subsequent configurations used previously converged restart files where possible. All 27 configurations were run 15k iterations before and after adaptation even though most all were converged much sooner. This scripting procedure allowed the matrix of cases to be run in a 'submit and forget' mode from the end of grid generation to the point of looking at the final post processed answers.

The solutions were run on single processors of an SGI R10000 16-processor computer. Each configuration required about 44 processor hours from start to finish. The 27 cases were submitted on a Friday afternoon with staggered start times over the weekend. The last case was completed on the following Tuesday.

RESULTS

Figure 5 shows Mach number and air mass fraction contours of the Draco internal flow path for two configurations, L/D=1, $A_s/A_p=1.5$ and $A_s/A_p=1$ and 3. The Mach number contours of the $A_s/A_p=3$ configuration indicate the primary flow attached to the mixer wall sooner and incurred significantly stronger shocks than the $A_s/A_p=1$ configuration. The shocks were caused by the primary flow's interaction with the secondary flow and the mixer wall. The Mach contours in the inlet show the $A_s/A_p=1$ configuration had a higher secondary flow rate.

In figure 5 the mixer exit plane is approximately one-third of the distance between the primary thruster exit and the engine exit. The air mass fraction contours indicate that at the mixer exit plane the $A_s/A_p=1$ configuration had slightly better mixing of the primary and secondary flows.

Figure 6 indicates the largest driver in the by-pass ratio was A_s/A_p . This was a result of the different primary thruster area ratios and, therefore, exit pressures. For the range of A_s/A_p studied the lowest primary thruster exit pressure ($A_s/A_p=1$) pumped the most secondary flow. Both L/D and A_8/A_5 had less dramatic but yet significant effects on by-pass ratio.

The ECR (figure 7) was lowest at $A_s/A_p=1$ because the high secondary flow rate diluted the average total pressure of the resultant mixed flow. ECR also was lowest for the largest L/D . This resulted from the increased number of shocks that occurred in the longer mixers.

The mixing efficiency (figure 8) shows that the $A_s/A_p=1$ configuration had the best mixed flow at the mixer exit. There was no significant difference between $L/D=2$ and 3. A_8/A_5 did not significantly effect mixing efficiency. Figure 9 plots the mixing efficiency for all configurations from the mixer inlet to the mixer exit plane. The $A_s/A_p=2$ and 3 decreased the mixing because of the higher primary thruster exit pressures compressed the secondary flow against the mixer walls.

In figure 10 the mixer thrust efficiency is shown versus axial station for the $L/D=3$ configurations. The mixer degraded thrust for all configurations. Note that A_8/A_5 has a significant effect on mixer thrust efficiency, especially for $A_s/A_p=1$.

CONCLUSIONS

In this trade study the $A_s/A_p=1$ configuration clearly had the highest by-pass ratios and mixer mixing efficiencies. The additional length of $L/D=3$ over $L/D=2$ did not significantly enhance the mixer mixing efficiency. The $A_8/A_5=1.5$ configurations had the highest mixer thrust efficiencies.

The CFD and related analysis tools are in place, working and streamlined for quick turn-around of Draco ejector/mixer configuration trade studies.

FUTURE WORK

If the PSU ejector benchmark determines that there is a better turbulence model for ejector flows than the $k-\epsilon$ model these 27 configurations will be re-run with the more appropriate turbulence model.

Response surface methodology⁶ will be incorporated into the solution procedure to determine optimum ejector/mixer configurations.

TRAILBLAZER

INTRODUCTION

The Trailblazer⁷ is a reusable, single-stage-to-orbit vehicle concept, intended to reduce the cost of space access by making optimum use of air-breathing propulsion. The Trailblazer is a hydrogen-oxygen fueled vertical take-off/horizontal landing vehicle with 130,000lb gross lift-off weight and 300lb payload. Figure 11 shows the Trailblazer reference vehicle. The propulsion system operates in four modes including ramjet, scramjet, and rocket modes from lift-off to orbit. A full description of the Trailblazer concept can be found in reference 7.

In scramjet mode the effective specific impulse is very sensitive to the expansion process efficiency, especially approaching the maximum air-breathing Mach number of about 10. To determine the expansion nozzle efficiency the Applied Fluid Dynamics Group is performing CFD analysis of the Trailblazer engine flowpath for the scramjet mode.

OBJECTIVE

The primary objective of this study is to provide estimates of the expansion process efficiency of the Trailblazer nozzle configuration in scramjet mode. The dominant loss mechanisms are to be identified and quantified in order to guide refinements in the nozzle design.

APPROACH

The analysis is being performed with the FDNS CFD code. Finite-rate chemistry and thermodynamics and standard k-ε turbulence model are implemented. The free-stream flow is included to accurately model the altitude compensating effect of the aft-body. Effects of vehicle angle of attack and yaw are neglected. Symmetry is assumed about a plane parallel to the vehicle axis that bisects the engine flowpath such that one half of an engine and 1/6th of the vehicle aft end are in the domain. Figure 12 shows the external portion of the computational domain. The engine inlet boundary conditions for the scramjet mode were provided by a one-dimensional engine performance code. The freestream velocity is set to Mach 10. The expansion process efficiency will be determined by post-processing the three-dimensional CFD solution of the nozzle flowfield

STATUS

Preliminary results are presented in terms of pressure contours in figures 13 through 15. Figure 13 shows the pressure contours along the plane of symmetry. Figures 14 and 15 show surface pressure contours in the neighborhood of the primary thruster and ramp respectively.

FUTURE WORK

After completion of the current scramjet mode analysis two additional engine modes will be analyzed; the ejector mode and the rocket mode. The primary objective will again be to determine the expansion process efficiency of the Trailblazer configuration.

ACKNOWLEDGEMENTS

The authors would like to thank Dr. C. Trefny and Mr. M. D'Agostino for their assistance with this work.

REFERENCES

1. Chen, Y. S., "FDNS - A General Purpose CFD Code, Version 4.0", Engineering Sciences, Inc., ESI-TR-97-01, Huntsville, AL., May 1997.
2. Lehman, M., Pal, S., Broda, J. C. and Santoro, R. J., "Raman Spectroscopy Based Study of RBCC Ejector Mode Performance," AIAA-99-0090, 37th AIAA Aerospace Sciences Meeting, Reno, NV, January 11-14, 1999.
3. Gridgen Version 13 user manual, <http://pointwise.com/>
4. Smith, S.D., "High Altitude Supersonic Flow of Chemically Reacting Gas-Particle Mixtures – Volume 1, LMSC-HREC TR D867400-1, Lockheed Missile and Space Company, Huntsville, AL., October 1984.
5. Davies, C. B. and Venkatapathy, E., "The Multidimensional Self-Adaptive Grid Code, SAGEv2", NASA TM 110350, April 1995.

6. Myers, R. H. and Montgomery, D. C., Response Surface Methodology-Process and Product Optimization Using Designed Experiments, John Wiley & Sons, 1995.
7. Trefny, C., "An Air-Breathing Launch Vehicle Concept for Single-Stage-to-Orbit", AIAA Paper 99-2730, June, 1999.

	L/D=1			L/D=2			L/D=3		
	As/Ap=1	As/Ap=2	As/Ap=3	As/Ap=1	As/Ap=2	As/Ap=3	As/Ap=1	As/Ap=2	As/Ap=3
A8/A5=1.5	1.1.15	1.2.15	1.3.15	2.1.15	2.2.15	2.3.15	3.1.15	3.2.15	3.3.15
A8/A5=2.	1.1.20	1.2.20	1.3.20	2.1.20	2.2.20	2.3.20	3.1.20	3.2.20	3.3.20
A8/A5=2.5	1.1.25	1.2.25	1.3.25	2.1.25	2.2.25	2.3.25	3.1.25	3.2.25	3.3.25

Table 1. Draco Ejector Cases

Figure 1. Penn State RBCC Ejector Mode Experimental Hardware

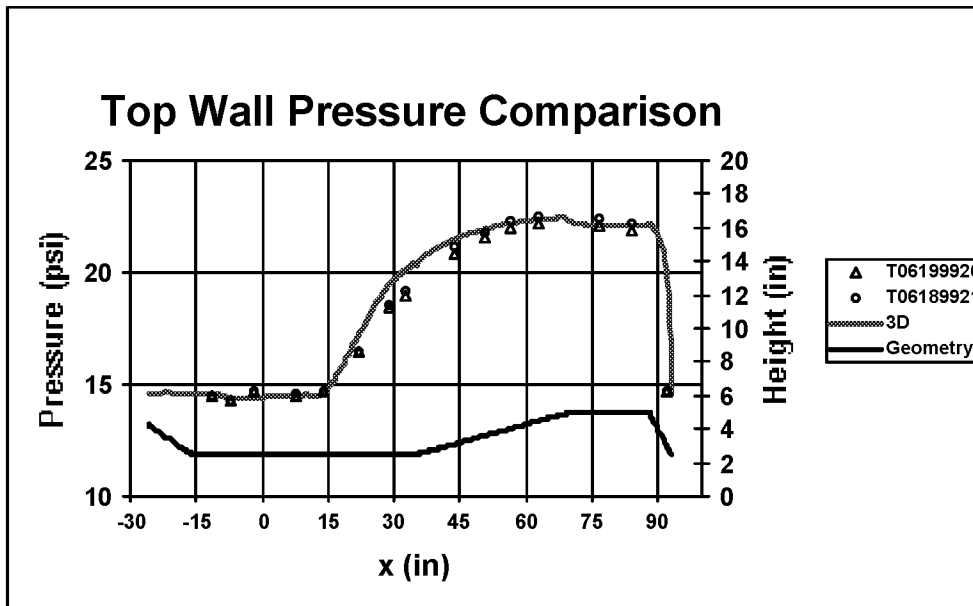
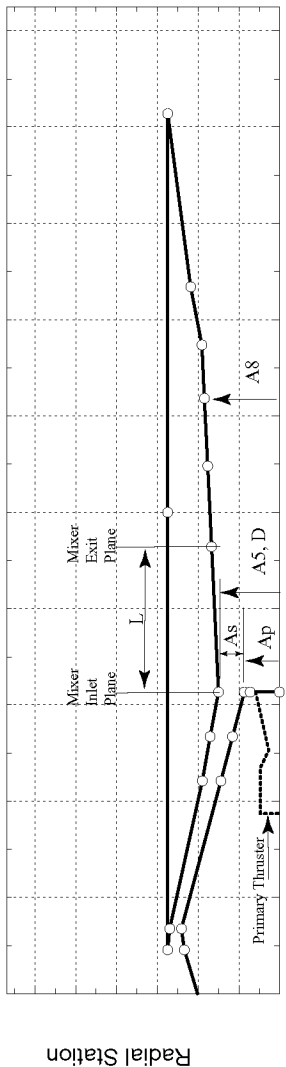


Figure 2. Comparison of FDNS and Test Data Upper Wall Pressures for Ejector Mode



Axial Station

A_s = Secondary Flow Area, Constant Area Inlet
 A_p = Primary Thruster Exit Area + Thruster Base Area
 $A_s/A_p = 1, 2$ or 3

L = Mixer Length
 D = Mixer Diameter at Inlet
 $L/D = 1, 2$ or 3

A_5 = Mixer Inlet Area
 A_8 = Ram Burner Area
 $A_8/A_5 = 1.5, 2.0,$ or 2.5

Figure 3. Draco Engine Layout

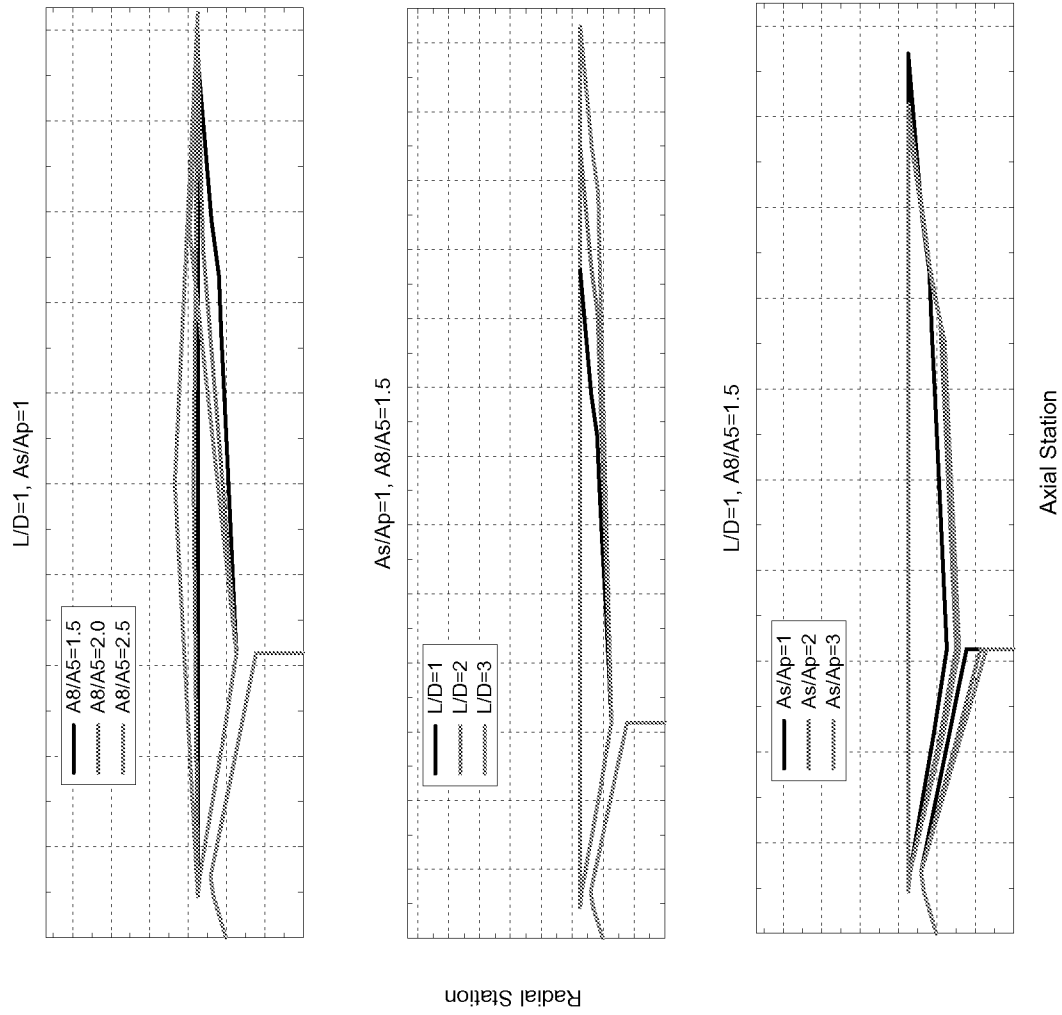
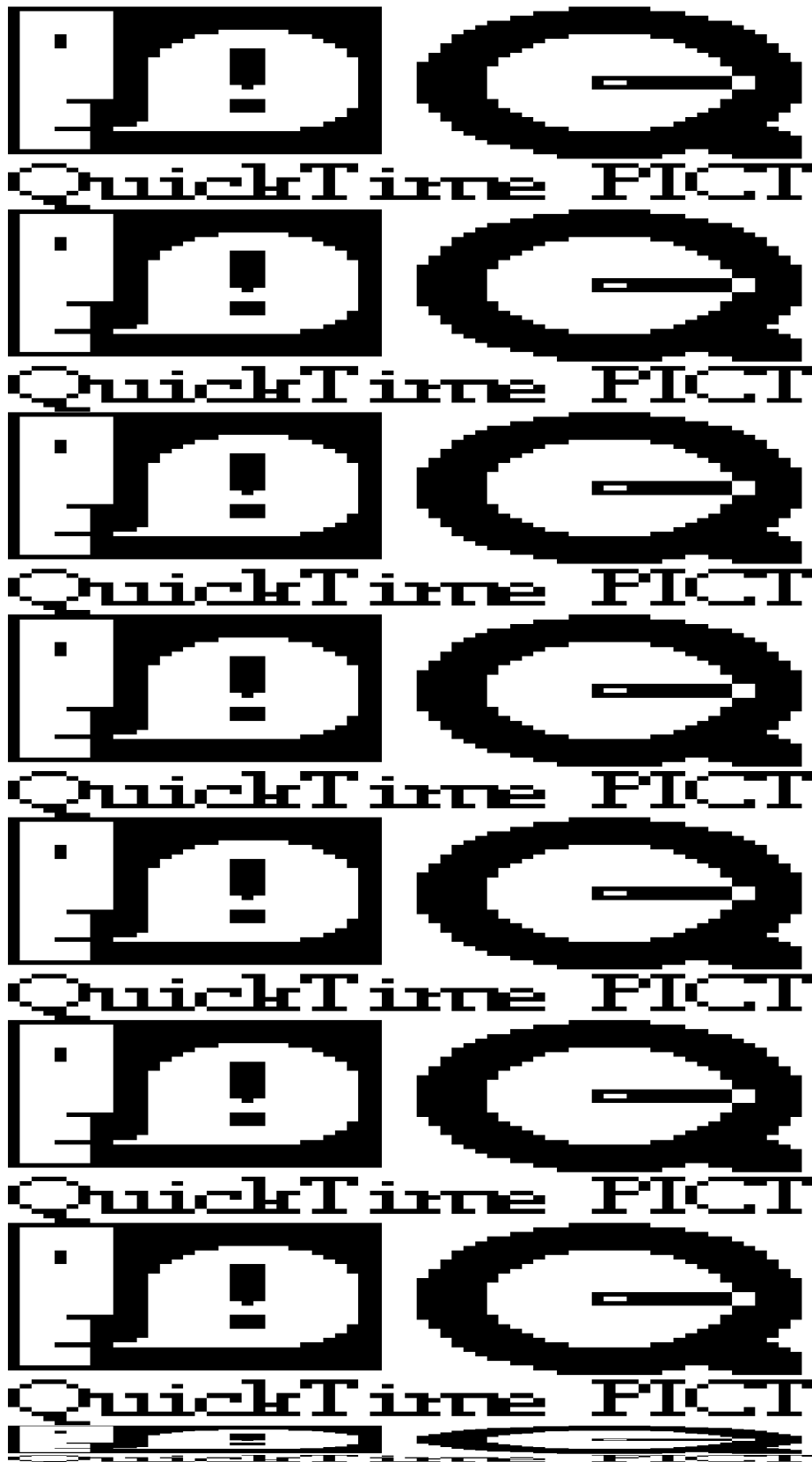


Figure 4. Examples of Engine Layouts in Trade Study



$L/D=1, A_8/A_5=1.5, A_9/A_p=3$

$L/D=1, A_8/A_5=1.5, A_9/A_p=1$

Figure 5. Mach and Mass Fraction Contours for $L/D=1, A_8/A_5=1.5, A_9/A_p=1$ and 3

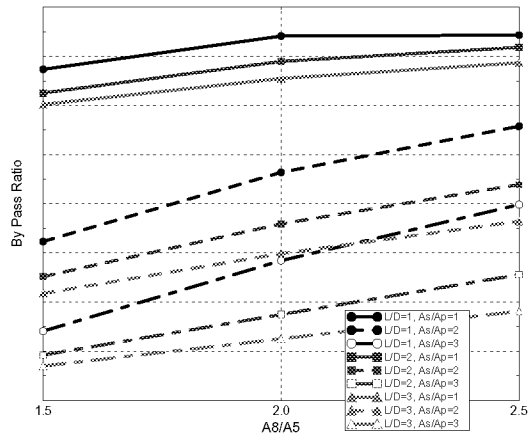


Figure 6. By-Pass Ratio vs. A_8/A_5

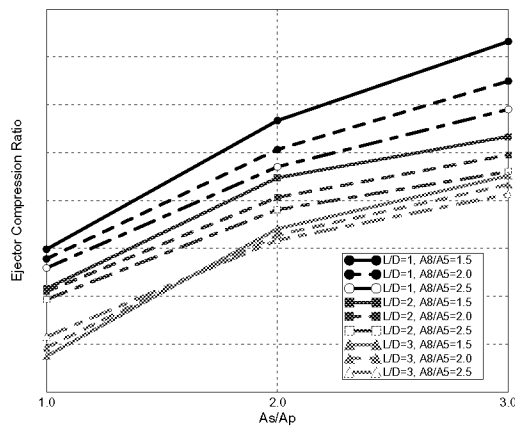


Figure 7. Ejector Compression Ratio vs. A_8/A_p

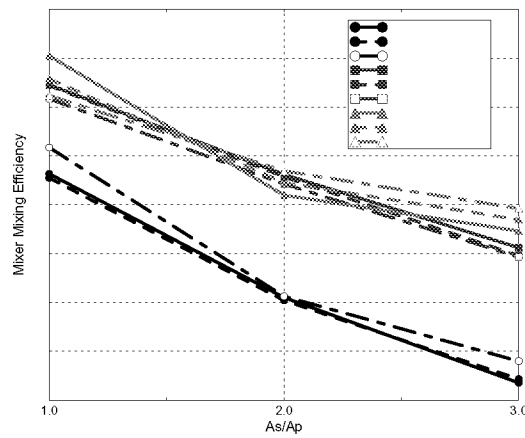


Figure 8. Mixer Mixing Efficiency vs. A_8/A_5

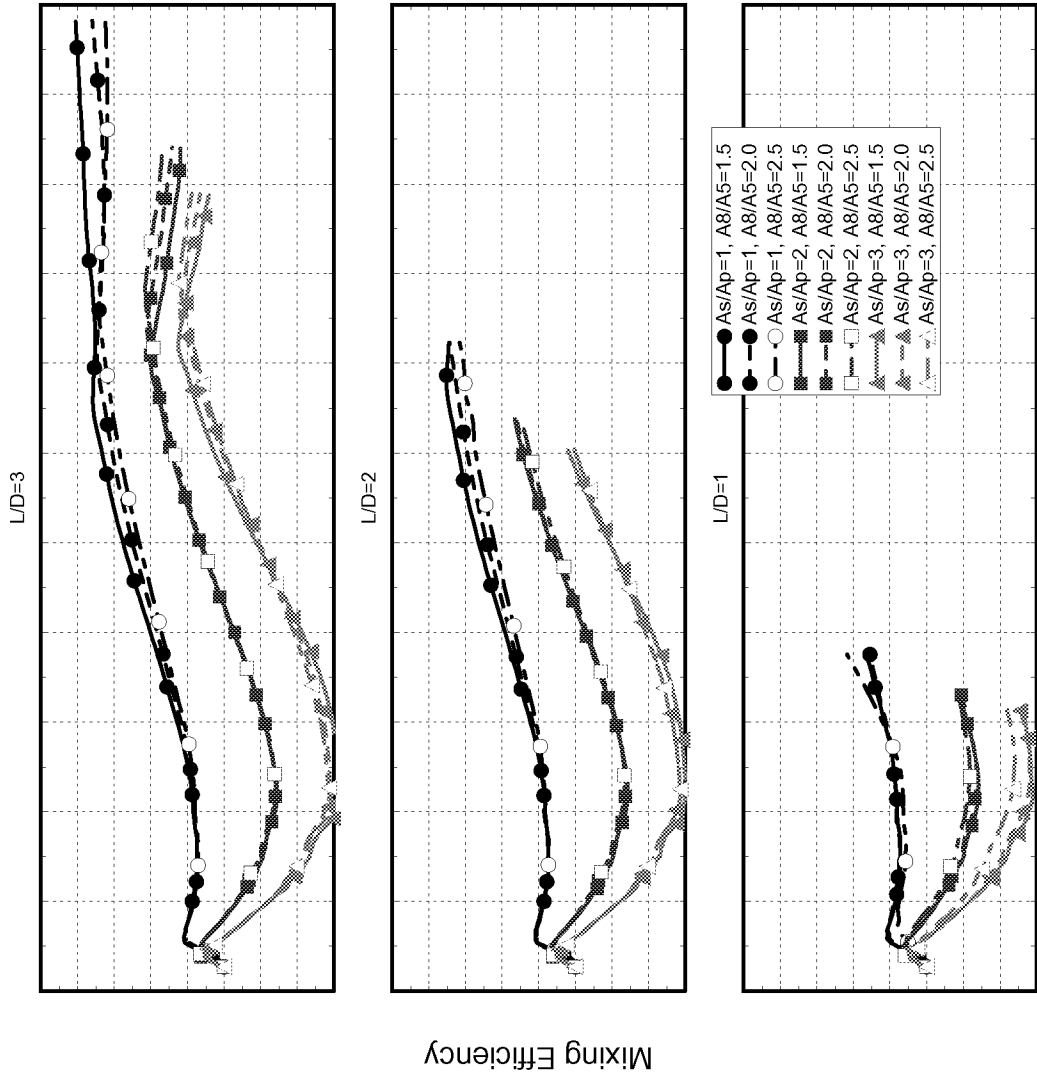


Figure 9. Mixer Mixing Efficiency vs. Axial Station

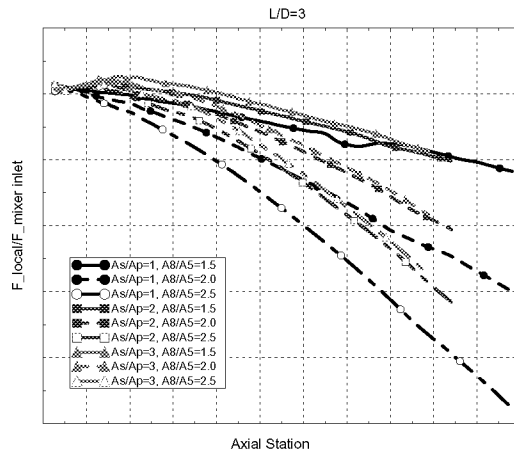


Figure 10. Mixer Thrust Efficiency vs. Axial Station for L/D=3 Configurations

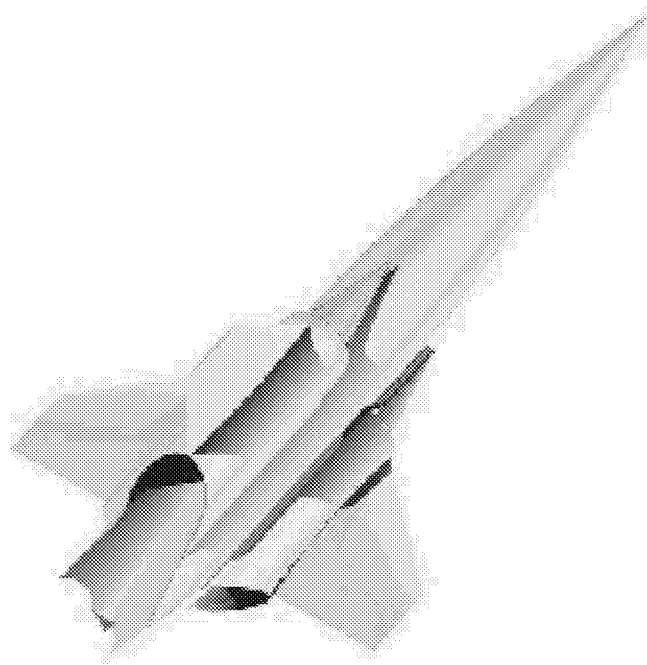


Figure 11. Trailblazer Reference Vehicle

Figure 12. Computational Domain for Trailblazer Nozzle Analysis

Pressure Contour

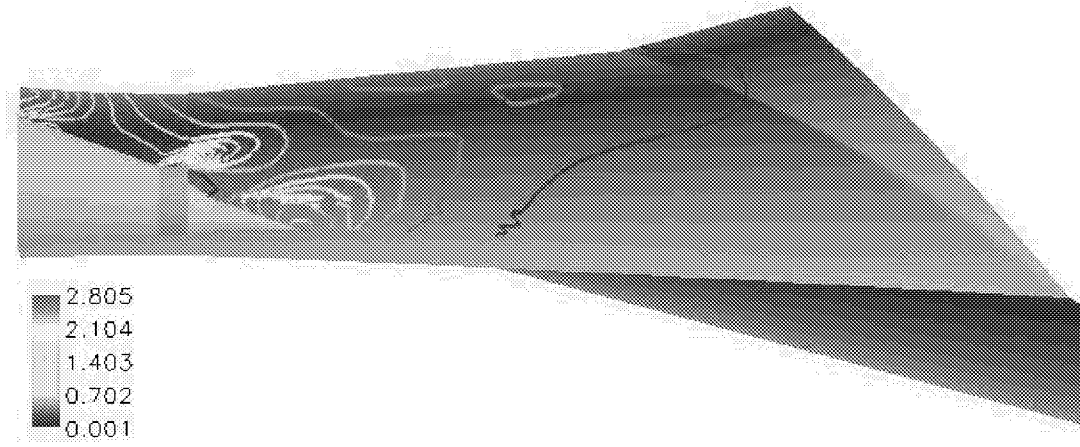


Figure 13. Pressure Contours on Symmetry Plane

Pressure Contour

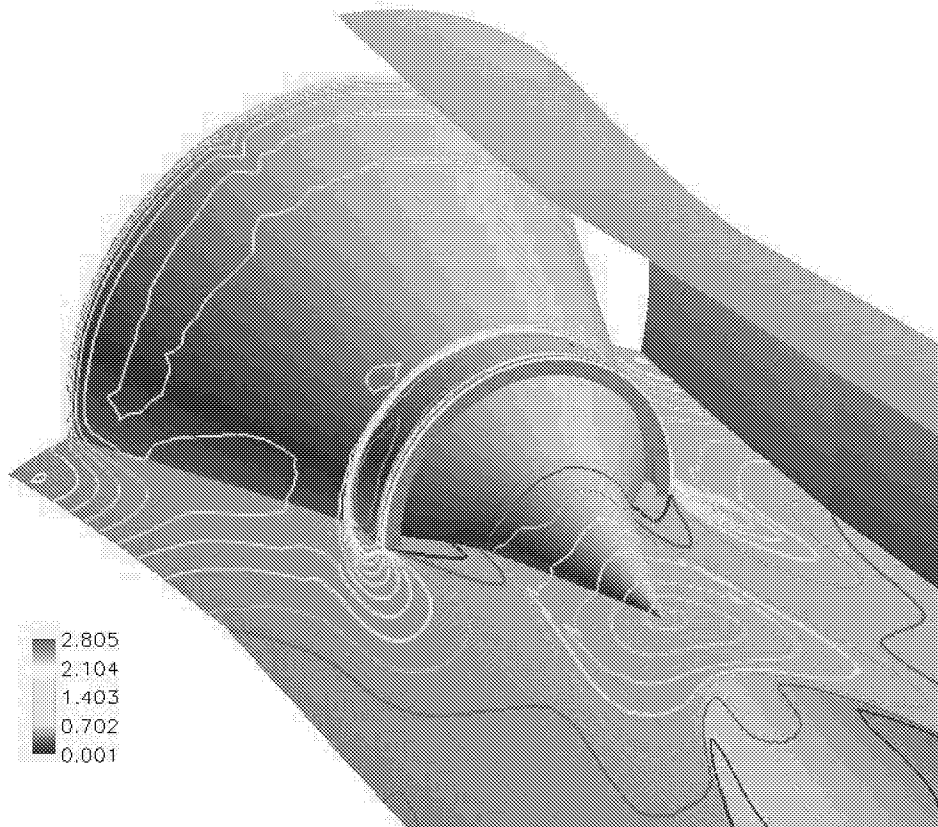


Figure 14. Pressure Contours Near Inlet and Primary Thruster

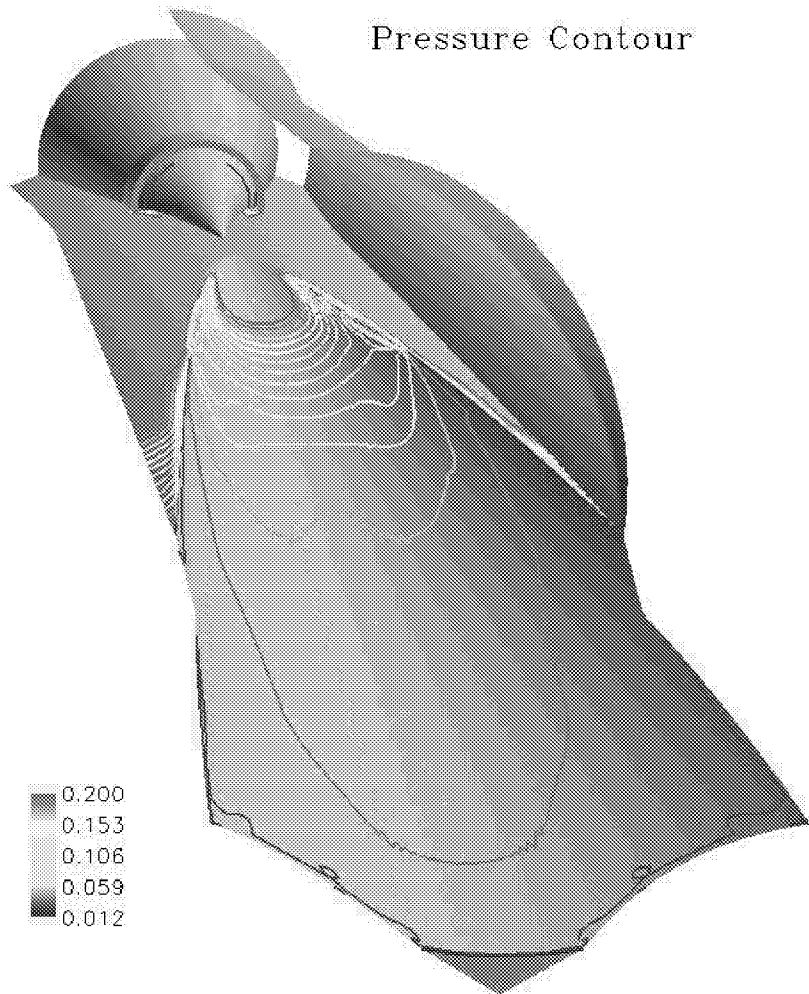


Figure 15. Pressure Contours on the Aft Ramp